Published in final edited form as:
Microcirculation. 2008 November ; 15(8): 795–811. doi:10.1080/10739680801938289.

Theoretical Models of Microvascular Oxygen Transport to Tissue

Daniel Goldman
Department of Medical Biophysics, 491 Medical Sciences Building The University of Western Ontario London, ON N6A 5C1 CANADA

Abstract

To improve understanding of microvascular O_2 transport, theoretical modeling has been pursued for many years. The large number of studies in this area attests to the complexities (biochemical, structural, hemodynamic) involved. This article focuses on theoretical studies from the last two decades and, in particular, on models of O_2 transport to tissue by discrete microvessels. A brief discussion of intravascular O_2 transport is first given, highlighting the physiological importance of intravascular resistance to blood-tissue O_2 transfer. This is followed by a description of the Krogh tissue cylinder model of O_2 transport by a single capillary, which is shown to remain relevant in modified forms that relax many of the original biophysical assumptions. However, there are many geometric and hemodynamic complexities that require the consideration of microvascular arrays and networks. Multi-vessel models are discussed which have shown the physiological importance of heterogeneities in vessel spacing, O_2 supply, red blood cell flow path, as well as interactions between capillaries and arterioles. These realistic models require sophisticated methods for solving the governing partial differential equations, and a range of solution techniques are described. Finally, the issue of experimental validation of microvascular O_2 delivery models is discussed, and new directions in O_2 transport modeling are outlined.

Keywords

capillary network; heterogeneity; computational model; spatially distributed; mathematical model

Introduction

To support the energy requirements of vertebrate tissues, oxygen is transported from the lungs to individual cells via the circulatory system. This O_2 is primarily carried in the form of oxyhemoglobin, i.e., bound to the hemoglobin (Hb) molecules inside red blood cells (RBCs). The actual transfer of O_2 from RBCs to parenchymal cells, where it is utilized by mitochondria, is accomplished in the microcirculation. Therefore, it is crucial to understand the transport properties of the microvasculature in order to understand both normal physiological function and a number of diseases that involve the microcirculation. However, there are a number of complexities that make microvascular O_2 transport difficult to study, particularly when quantitative results are desired. The microvasculature has a very complicated three-dimensional spatial structure and a small scale (~1–100μm). Its structural complexity leads to heterogeneity in microvascular perfusion, and unique hemodynamic effects not seen in larger vessels (e.g., substantial variations in hematocrit) occur due to the fact that many vessel sizes are on the order of the RBC size. RBC perfusion heterogeneity in turn leads to heterogeneities in O_2 supply, tissue oxygenation, and O_2 consumption. These heterogeneities can have important physiological consequences (e.g., localized hypoxia), but

dgoldma2@uwo.ca, Phone: 519-661-2111-x80213, Fax: 519-661-2123.

since they are difficult to characterize experimentally (64), theoretical modeling has been used to study their effects. This theoretical work began with Krogh and Erlang (49), and was taken up again in the 1960s. The various aspects of steady-state and time-dependent O_2 transport that have been studied up to the late 1980s, from Hb-O_2 binding to whole-organ transport, were discussed very thoroughly by Popel (65). Here we mainly consider theoretical models of O_2 transport that have been used since that time and, in particular, concentrate on spatially distributed models at the level of single and multiple discrete microvessels. For the most part, compartmental models (e.g., (78)), models using continuous vessel descriptions (e.g., (71)), and models in artificial tissues (e.g., (82)) are not considered, and the focus is on tissue O_2 transport in skeletal muscle, heart, brain, and tumors. Both theoretical models and the results they were used to obtain are discussed.

This article begins with a brief discussion of intraerythrocyte and intravascular O_2 transport (see (65) and (34) for more details), including factors that determine intravascular resistance to blood-tissue O_2 transport. The original Krogh model of O_2 delivery by a single capillary is then presented and its main assumptions are listed. The importance of these is discussed; first in the context of single-vessel models (including time-dependent and multi-species cases), and then in terms of models that use multi-vessel arrays or networks and require sophisticated analytical or numerical solution techniques. Finally, experimental support for realistic modeling of microvascular O_2 transport and new directions in modeling are discussed.

Intraerythrocyte and Intravascular Transport Models

Red Blood Cells

Since most O_2 is carried in the blood bound to hemoglobin (Hb) inside red blood cells (RBCs), realistic modeling of microvascular O_2 transport requires a model of Hb-O_2 binding. This binding occurs in four steps, due to the fact that the Hb molecule has four O_2 binding sites (heme groups) that act cooperatively. A full description of the equilibrium binding (for models of Hb-O_2 binding kinetics, see (65)) therefore requires four experimental constants and is given by the Adair equation. However, the Adair equation cannot be inverted analytically, so the easily invertible Hill equation has been used in most theoretical models to describe fractional Hb-O_2 saturation (SO_2):

$$S(P)=\frac{P^n}{P^n+P_{50}^n} \qquad (1)$$

(1)

Here P is the local O_2 partial pressure (PO_2) inside the RBC, P_{50} is the half-saturation PO_2 and *n* is the Hill exponent. P_{50} and *n* are obtained by fitting the Hill equation to experimental data on the oxyhemoglobin dissociation curve, with typical values of P_{50}=29mmHg and *n*=2.2 for hamster (17) and P_{50}=37mmHg and *n*=2.7 for rat (15). The Hb-O_2 dissociation curve given by Eq. (1) is shown in Fig. 1. Although the Hill equation is only highly accurate in the SO_2 range of 20–80%, this has been deemed sufficient for most O_2 transport models, given the other approximations used. Note that the exact form of the dissociation curve (e.g., P_{50} and *n*) varies with blood pH, CO_2 concentration, concentration of 2,3-diphosphoglycerate (DPG), and temperature. A useful model of this dependence was recently described (12); see appendix of (13) for errata.

The amount of Hb-bound O_2 at any point inside a RBC is given by C_{Hb} S, while the amounts of free or dissolved O_2 in the RBC and the plasma are given by α_{RBC} P_{RBC} and α_{pl}

P_{pl}, respectively, where α_{RBC} and α_{pl} are O_2 solubilities and P_{RBC} and P_{pl} are PO_2 values. The total concentration of free and Hb-bound O_2 in a given blood sample is

$$\alpha_{pl}P_{pl}(1-H)+\alpha_{RBC}P_{RBC}H+C_{Hb}SH \tag{2}$$

where P_{pl} and P_{RBC} are the average PO_2 values in the plasma and RBCs, H is the hematocrit, C_{Hb} is the O_2-binding capacity of RBC Hb solution, and S is the average SO_2 inside the RBCs. Note that here C_{Hb} is the product of the RBC hemoglobin concentration and the O_2 binding capacity of Hb. In addition to describing Hb-O_2 binding and blood O_2 concentration, understanding O_2 transport also requires modeling the diffusion of free and Hb-bound O_2 within the RBC and the transport of O_2 through the cell membrane. Theoretical work of this type has been performed in the past (see (65)); however, more recently RBC-plasma O_2 transport models have been incorporated into intravascular O_2 transport models, as described below.

Capillaries

In order to model O_2 transport from capillary blood to tissue, it is necessary to consider the properties of O_2 transport inside capillaries. Many models (including Krogh-Erlang) that have focused on O_2 transport in the tissue surrounding capillaries have failed to account for intracapillary O_2 gradients, which lead to an effective resistance to blood-tissue O_2 transport (34). To quantify capillary intravascular resistance (IVR), theoretical studies have been performed to determine the magnitude of this resistance and how it depends on various parameters such as capillary diameter and RBC velocity.

Following earlier work (see (34)), Federspiel and Popel (18) considered stationary spherical RBCs arranged in single file with a full description of diffusion of free and Hb-bound O_2 inside the RBCs, the kinetics of Hb-O_2 binding, and diffusion of O_2 in the surrounding plasma. Using a constant PO_2 at the capillary wall, it was shown that the mass transfer coefficient (MTC) or inverse resistance depends strongly on hematocrit (or the inverse of the RBC spacing) and also on capillary diameter relative to RBC size (clearance). The MTC was several times smaller for discrete RBCs than for a continuous Hb solution, and application to a capillary-tissue transport model implied IVR was 30–70% of the total resistance for O_2 transport from blood to tissue. A subsequent study (92) showed that RBC shape affects O_2 flux, with calculated MTC increasing by 26% as the RBC changed from its undeformed disc shape to parachute shape.

The capillary MTC is usually defined as the average flux of O_2 per unit area through the capillary wall divided by the average difference between intraerythrocyte PO_2 and wall PO_2:

$$k_{cap}=\frac{\langle j_{wall}\rangle}{\left\langle P_{cap}-P_{wall}\right\rangle} \tag{3}$$

The MTC can be expressed in dimensionless form as a Nusselt number:

$$Nu=\frac{\langle j_{wall}\rangle R_{cap}}{\left\langle P_{cap}-P_{wall}\right\rangle D_{pl}\alpha_{pl}} \tag{4}$$

where R_{cap} is the capillary radius, and D_{pl} and α_{pl} are the plasma O_2 diffusivity and solubility, respectively. Capillary diameter and RBC O_2 diffusivity and solubility can also be used to obtain Nu from *k*, and P_{cap} can be replaced with P*, the PO_2 based on the average RBC SO_2.

Groebe and Thews (31) used a finite-difference method to study O_2 transport from moving cylindrical RBCs (without plasma convection) in heavily working muscle for O_2 flux and PO_2 boundary conditions at the wall. Increased RBC spacing decreased overall capillary O_2 release but increased release by individual RBCs, and it was concluded that O_2 flux oscillations due to RBC movement did not significantly affect tissue O_2 delivery. Bos et al. (7) presented a model of intravascular O_2 transport that used point sources to represent discrete RBCs and a tissue cylinder surrounding the capillary with constant O_2 consumption and Mb facilitation. A “stroboscopic” method was used to follow equally spaced RBCs as they moved through a capillary at constant velocity. Although resistance due to plasma, capillary wall, and interstitium was not considered, the model allowed calculation of a PO_2 drop between the RBC center and the capillary wall and hence estimation of the effective PO_2 drop (extraction pressure, EP) between capillary and tissue due to intravascular gradients. EP was shown to vary from about 4–20mmHg as hematocrit decreased from 50-20% and to decrease slightly towards the venous end of the capillary. Bos et al. (6) studied transport from cylindrical RBCs with plasma and tissue layers using a finite-difference method. The results of the point-source model were generally confirmed, and behavior of EP was determined for a range of hematocrits and Peclet numbers ($Pe=v_{RBC}l/D$, where l is the RBC spacing and D is the plasma O_2 diffusivity). Over the same range of parameters, plasma convection only changed EP by approximately 10% or less.

More recently, capillary MTCs for O_2 have been computed using models that include separate concentric layers surrounding the lumen to represent the capillary wall, interstitial space, and parenchymal tissue (Fig. 2). Using cylindrical RBCs, Eggleton et al. (14) calculated MTCs for hematocrits of 25–55% and showed only a weak dependence on RBC velocity and capillary radius. This work also demonstrated that assuming a constant wall PO_2, instead of using an actual model of O_2-consuming tissue, results in a significant overestimate of the MTC, as does using the Clark approximation (10) for RBC-plasma O_2 flux. A quadratic equation was given that closely fit the computed dependence of the MTC on hematocrit:

$$k_{cap}=1.21-4.38H+23.6H^2\ (\mathrm{nlO_2 s^{-1} mmHg^{-1} cm^{-2}}) \tag{5}$$

However, it was not clear how accurate this equation would be for capillary hematocrits below 25%, as are often seen experimentally. A model similar to (14) but with the addition of plasma convection was used to compute MTCs (for capillary-tissue and RBC-plasma transport) when a Hb solution was present in the plasma (88). MTCs in this case depended on both hematocrit (in the range 20%-40%) and SO_2. Hb-O_2 binding kinetics had a relatively small effect (<20%) on MTCs for normal blood, but a much larger effect (~55%) in the presence of plasma Hb.

Arterioles and Venules

Since arterioles are also involved in blood-tissue diffusive O_2 transport, it is important to understand how they carry O_2 and release (or take up) O_2 to the surrounding tissue before including them in models of tissue O_2 delivery. As pointed out by Hellums et al. (34), there are two distinct size regimes of non-capillary microvessels that must be considered. In larger microvessels (20–100μm diameter), intravascular O_2 transport can be modeled using a continuum RBC distribution in the vessel core surrounded by a plasma layer. However, in smaller microvessels (8–15μm), it is believed that the actual distribution of RBCs in the lumen needs to be considered to accurately predict O_2 transport properties. No theoretical work has yet been done on this latter case, due to the geometric and computational complexities involved, and therefore only extrapolations from results for smaller and larger vessels are available.

For 20–100μm vessels, Nair et al. (59) developed a theoretical model of intravascular O_2 transport and validated it against experimental data. This model utilized assumed hematocrit and velocity distributions inside the vessel and a finite-element method to calculate steady-state O_2 transport in the RBC-rich core and plasma sleeve regions, which were coupled by assuming continuity of PO_2. This model included Hb-O_2 kinetics and transport between the RBCs and plasma in the core. A simplified model (60) assumed equilibrium Hb-O_2 binding and equilibrium between the plasma and RBC Hb in the core, and both models agreed well with O_2 saturation measurements in a 27μm artificial capillary. These models were used to calculate MTCs for diameters in the range 15–100μm. While MTCs generally depend only weakly on SO_2 in capillaries, they increase approximately linearly with SO_2 in arterioles, and the slope of this relation increases with increasing vessel diameter. Huang and Hellums (41) presented a model of coupled O_2/CO_2 transport inside a large microvessel. This model included many of the same properties as (60), but also contained a detailed description of the complex process of CO_2 transport and its effect on O_2 transport. It was shown that the two-phase nature of blood (plasma and RBCs) and deviations from local chemical equilibrium needed to be considered to accurately predict blood O_2 release accompanied by CO_2 uptake.

Page et al. (61) extended the model (59) to the case where a Hb solution was present in the plasma and included a new treatment of shear augmentation, which was more important than for the case without plasma Hb (particularly for O_2 uptake). This model was shown to agree with experimental data on O_2 release and uptake in a 25μm artificial capillary. An interesting result of this work was that blood containing RBCs and 30% Hb solution had the same O_2 transport capability as an Hb solution without RBCs having the same total Hb content. A similar model but with O_2 flux boundary conditions was recently presented by Cole et al. (11). While the above models of Hellums and co-workers were validated in terms of overall change in O_2 content, it was not possible to validate the details of intravascular transport of O_2, and the possible effects of the vascular wall, interstitial space, and surrounding tissue were not considered.

Note that, up to the present time, there have been a number of limitations on the degree to which microvascular O_2 transport (geometry, hemodynamics, O_2 concentration) could be studied experimentally. Although three-dimensional data is required, the length scales involved (<100μm) have been too small for *in vivo* imaging modalities such as magnetic resonance (MRI), x-ray tomography (CT), and ultrasound (US). Sectioning and electron microscopy of *ex vivo* tissue samples allow three-dimensional geometry to be obtained; however, microvessel O_2 supply rates (RBC supply rate and SO_2) cannot be obtained, and true *in vivo* geometry can be lost due to sample shrinkage or unphysiological vasodilation. Therefore, intravital videomicroscopy (43) has been the principal technique used, although it too has limitations in terms of the depth at which measurements can be made (typically <100μm), the amount of three-dimensional information that can be obtained, its temporal resolution (and hence maximum RBC velocity as well as minimum intravascular length scale), and its accuracy and spatial resolution in determining RBC SO_2 values (16) and plasma or tissue PO_2 values (26,27). Experimental uncertainties in vessel-tissue geometry, intra- and perivascular O_2 distributions, and hemodynamics (e.g., RBC supply distributions), as well as in *in vivo* parameters such as maximal O_2 consumption rate and O_2 diffusivity, have motivated much of the theoretical modeling that has been performed on microvascular O_2 transport. This modeling has made possible investigation of fundamental biophysical effects that could not be studied experimentally, such as the role of plasma convection in capillary-tissue transport (6), and has proven very valuable in supplementing experimental data, such as in calculating three-dimensional tissue PO_2 distributions from measured capillary geometry and hemodynamics (23).

Single-Vessel (Tissue Cylinder) Transport Models

Standard Krogh Model

A natural way to begin studying blood-tissue O_2 transport is to consider a single blood vessel and its release of O_2 into the surrounding tissue. Inspired by the structure of skeletal muscle, with its parallel muscle fibers and capillaries, Krogh (49) originated the idea of representing the O_2 transport in an entire microvascular bed by a single capillary that supplies O_2 to the cylinder of tissue surrounding it. This axisymmetric (tissue cylinder) geometry, with a number of additional assumptions, is known as the Krogh model. The prediction of this model for tissue PO_2 was obtained by Krogh with the assistance of the mathematician Erlang, hence the result is known as the Krogh-Erlang solution. The additional assumptions of this model, some of which were not explicit at the time it was proposed, are:

1. Tissue O_2 consumption is constant and uniform
2. Tissue PO_2 at the capillary wall equals average capillary PO_2 (no IVR)
3. Tissue O_2 solubility and diffusivity are uniform
4. Axial (or longitudinal) diffusion of O_2 is not significant
5. All important microvascular O_2 transport phenomena are steady-state
6. All capillaries are parallel, unbranched, and equally spaced
7. All capillaries receive equal convective O_2 supply (RBC supply rate times entrance SO_2)
8. Capillaries are the only microvessels that play a role in O_2 transport to tissue

The above assumptions lead to the following reaction-diffusion problem for steady-state PO_2 in the tissue cylinder (P), given capillary PO_2 (P_{cap}):

$$D\alpha \frac{1}{r}\frac{\partial}{\partial r}\left(r\frac{\partial P}{\partial r}\right)=M_0 \quad \text{with } P=P_{cap} \text{ at } r=R_{cap} \text{ and } \partial P/\partial r=0 \text{ at } r=R_t \tag{6}$$

where r is the radial coordinate, D is the tissue O_2 diffusivity, α is the tissue O_2 solubility, M_0 is the tissue O_2 consumption rate, R_{cap} is the capillary radius, and R_t is the tissue radius. The Krogh diffusion coefficient is defined as K=Dα. The solution (Krogh-Erlang) to the above equation is:

$$P(r)=P_{cap}+\frac{M_0}{4D\alpha}\left(r^2-R_c^2\right)-\frac{M_0R_t^2}{2D\alpha}\ln\frac{r}{R_{cap}} \tag{7}$$

Thus, given a small number of geometric (R_{cap}, R_t) and biophysical (D, α, M_0) parameters and P_{cap} at a given location, the Krogh model is able to predict the radial variation in tissue PO_2, including the minimum PO_2, which occurs at the outer edge of the tissue cylinder ($r=R_t$).

By supplementing the above model with a cross-sectionally averaged model of capillary O_2 transport, it is possible to predict the PO_2 in a capillary and its surrounding tissue.

Neglecting O_2 dissolved in the plasma, intracapillary transport can be described by the following convection problem for capillary SO_2 (S), given capillary entrance SO_2 (S_a):

$$\pi R_c^2 H C_{Hb} v \frac{\partial S}{\partial z} = -2\pi j(z) R_c \text{ with } S = S_a \text{ at } z=0 \tag{8}$$

where H is capillary hematocrit, C_{Hb} is the O_2-binding capacity of the RBC Hb solution, v is RBC velocity, and j is O_2 flux per unit area leaving the capillary at axial location z. Since the Krogh model assumes constant O_2 consumption and no axial diffusion, the O_2 flux for all z is:

$$j(z) = -D\alpha \frac{\partial P}{\partial r}\Big|_{R_c} = \frac{M_0}{2R_c}\left(R_t^2 - R_c^2\right) \tag{9}$$

This result allows direct integration of the capillary transport equation to obtain the solution:

$$S(z) = S_a - \frac{M_0\left(R_t^2 - R_c^2\right)}{H C_{Hb} v} z \tag{10}$$

Given an invertible form of the Hb-O_2 dissociation curve (e.g., the Hill equation), Eq. (10) gives $P_{cap}(z)=P(S(z))$ at each axial location, which can be used in the solution (7) for tissue PO_2. The minimum tissue PO_2 for the above capillary-tissue model occurs at z=L (capillary exit) and $r=R_t$ (the “lethal corner”). Although its predictions for tissue PO_2 generally differ from experimental measurements, the Krogh model remains an important starting point for understanding O_2 transport to tissue. It represents the case of perfectly homogeneous O_2 transport, and for capillary transport with unidirectional flow gives the largest minimum tissue PO_2 and least tissue PO_2 heterogeneity (coefficient of variation or relative dispersion, =(standard deviation)/mean).

Modified Krogh Models

In an attempt to improve the physiological accuracy of the Krogh model, and to better match experiment, a number of modifications have been incorporated into the model. The most important modifications made while maintaining the Krogh geometry include (c.f. assumptions 1–5 above): variable (PO_2-dependent) tissue O_2 consumption, IVR to O_2 transport or a model of intravascular O_2 gradients, facilitated diffusion by tissue myoglobin (Mb), axial O_2 diffusion in the tissue, and time-dependent transport.

i. PO_2-Dependent O_2 Consumption—Experimentally, the local tissue O_2 consumption rate is found to be approximately constant for tissue PO_2 above a certain critical value, P_{crit}; below this value O_2 consumption drops off sharply to zero (possibly due to diffusion limitation of O_2 flux into mitochondria). Therefore, in order to study situations in which hypoxia is expected, a mathematical model of PO_2-dependent consumption is required. The most common model (Michaelis-Menten) uses first-order kinetics and gives the following equilibrium O_2 consumption rate:

$$M(P) = \frac{M_0 P}{P + P_{crit}} \tag{11}$$

where P is the tissue PO_2 and M_0 is the maximum local O_2 consumption rate. The Michaelis-Menten model does not keep O_2 consumption strictly constant for $P>P_{crit}$, but gives a reasonable approximation to the actual behavior and is more convenient computationally than the zeroth-order ("on/off") model. Although M_0 depends on the particular tissue and conditions being considered, P_{crit} is usually taken to be in the range 0.5–1.0 mmHg. Tissue O_2 consumption is often assumed to be uniform, but mitochondrial clustering has been considered in some models (28,58).

ii. Intravascular O_2 Transport Resistance—As discussed above, the existence of intravascular PO_2 gradients implies a finite IVR to blood-tissue O_2 transport. In a number of models of O_2 transport to tissue (see above), intravascular O_2 transport is directly included. However, when this approach is not desirable (e.g., for network problems where the computational cost would be too high), MTCs computed separately can be included in the vessel-tissue transport problem. This is typically done by using a flux boundary condition on tissue PO_2 at the outer edge of the microvessel wall instead of the continuous PO_2 condition of the Krogh model:

$$-D\alpha\frac{\partial P_w}{\partial r}=j_{wall}\equiv k\left(P_{cap}-P_w\right) \tag{12}$$

where j_{wall} is the capillary-tissue O_2 flux, k is the MTC, P_w is the tissue PO_2 at the vessel wall, and P_{cap} is the cross-sectionally averaged intravascular PO_2.

iii. Mb Facilitation of O_2 Diffusion—The Mb molecule found in heart and striated muscle can bind and release O_2 in the same way as Hb, and its movement can enhance O_2 diffusion. Since Mb has only one heme group, there is no cooperativity of binding and the equilbrium Mb-O_2 dissociation curve is given by:

$$S_{Mb}(P)=\frac{P}{P+P_{Mb,50}} \tag{13}$$

where $P_{Mb,50}$ is the experimentally determined half-saturation value. Using Fick's law, the flux of O_2 bound to Mb can be expressed as $j_{Mb02}=-D_{Mb}\,C_{Mb}\,\nabla S_{Mb}$, where D_{Mb} is the Mb diffusion coefficient (assumed the same for free and O_2-bound Mb) and C_{Mb} is the total O_2 binding capacity of tissue Mb. Expressing the total O_2 flux as $j=-D\alpha\nabla P-D_{Mb}C_{Mb}\nabla S_{Mb}$ and using the above expression for $S_{Mb}(P)$, we obtain

$$j=-D\alpha\left(1+\frac{D_{Mb}C_{Mb}}{D\alpha}\frac{P_{Mb,50}}{\left(P+P_{Mb,50}\right)^2}\right)\nabla P \tag{14}$$

where the second term inside the parentheses represents the increase in the effective O_2 diffusion constant due to Mb facilitation. Since $P_{Mb,50}$ is relatively small (~2–5mmHg), this facilitation will only be significant at low PO_2 values, i.e., when the Mb-O_2 dissociation curve (Fig. 1) has a significant slope. The above expression for j can be used to obtain a steady-state equation for tissue O_2 diffusion and consumption by setting $-\nabla\cdot j=M$, where M is the O_2 consumption rate. Mb gives tissue some resistance to localized hypoxia by increasing diffusion to low-PO_2 regions, and also plays a role in local O_2 storage and buffering. Mb diffusion appears to be isotropic in heart and skeletal muscle cells (62) with $D_{Mb}\approx 8\times10^{-7}\,cm^2/s$ in heart at 40°C (55).

iv. Axial O_2 Diffusion in the Tissue—This feature has also been found to be important in modeling microvascular O_2 transport, because each slice of the tissue cylinder is not independent but can exchange O_2 with its neighbors. Axial diffusion inside flowing microvessels is less important due to the relatively greater effect of axial convection. This can be quantified with a Peclet number, Pe=*v*L/D, which represents the importance of transport by convection (proportional to blood or RBC velocity *v*) relative to transport by diffusion (proportional to D/L for diffusion coefficient D and length scale L). For a typical capillary RBC velocity of 200μm/s and length of 500μm, and a typical diffusivity of 4×10^{-5}cm^2/s, we have Pe=25. This number will be larger in arterioles and venules, and therefore axial diffusion can be neglected inside most flowing microvessels. Adding axial diffusion to the Krogh model simply requires an additional $D\alpha\, \partial^2 P/\partial z^2$ term on the left-hand side of Eq. (3). Fig. 3 shows how neglecting each of the preceding four properties affects capillary and tissue PO_2 in the Krogh geometry.

v. Time-Dependent O_2 Transport—The convective O_2 supply to individual capillaries can vary considerably over time (e.g., due to upstream arteriolar vasomotion), and there are many problems of interest in which time-dependent O_2 transport is relevant (e.g., the onset of ischemia or exercise). Therefore, several studies have used time-dependent Krogh-type models. The necessary mathematical description involves the time-dependent forms of Eqs. (6) and (8), with appropriate initial and external boundary conditions, and a capillary-tissue interface condition as in Eq. (12). For example, with features i–iv above, tissue PO_2 can be described by

$$\frac{\partial P}{\partial t}=\left[1+\frac{C_{Mb}}{\alpha}\frac{dS_{Mb}}{dP}\right]^{-1}\left\{D\nabla^2 P-\frac{1}{\alpha}M(P)+\frac{1}{\alpha}D_{Mb}C_{Mb}\nabla\cdot\left(\frac{dS_{Mb}}{dP}\nabla P\right)\right\} \tag{15}$$

where ∇^2 includes both *r* and *z* derivatives. Capillary SO_2 can be described by

$$\frac{\partial S}{\partial t}=-\left[HC_{Hb}+\alpha_b\frac{\partial P_b}{\partial S}\right]^{-1}\left\{v_b\left(H_D C_{Hb}+\alpha_B\frac{\partial P_b}{\partial S}\right)\frac{\partial S}{\partial z}+\frac{2}{R}j_{wall}\right\} \tag{16}$$

where α_b and α_B are the volume- and flow-averaged blood O_2 solubilities, v_b is the average blood velocity, H_D is the discharge (flow-weighted) hematocrit, j_{wall} is the capillary wall flux per unit area given by Eq. (12), and $P_b(S)$ is the average blood PO_2 given by the inverted form of Eq. (1). This model includes dissolved PO_2 in the blood and assumes that average plasma and RBC PO_2 at each axial location are approximately equal.

Schumacker and Samsel (73) used a Krogh model with PO_2-dependent consumption (constant above 1mmHg, zero below) to analyze O_2 delivery and tissue uptake. Using reduced hematocrit, capillary entrance SO_2, or RBC velocity to decrease tissue O_2 supply, they investigated the role of diffusion limitation in the supply dependency of tissue O_2 extraction. It was found that the critical O_2 supply (at which O_2 uptake begins to decrease) was the same for all three types of hypoxia as long as the tissue cylinder radius was less than 80μm (for the assumed O_2 consumption rate). However, this led to critical O_2 extraction ratios (O_2 uptake divided by O_2 supply) greater than 90%, whereas experimental values are in the 65–75% range. In order to match both the measured critical extraction ratios and the observed similarity between the three types of hypoxia, it was necessary to assume a 30% functional O_2 shunt. These results demonstrated the limitations of the Krogh model in trying to analyze situations in which transport heterogeneity is important. Using Krogh and Hill (uniform O_2 supply on exterior of tissue cylinder) models, Piiper and Scheid (63) performed a similar study and showed that if multiple size tissue cylinders were considered (simulated supply heterogeneity), diffusion limitation began at a lower O_2 supply than in a single cylinder with the same average diameter.

Lagerlund and Low (51) used a Krogh-type model with axial diffusion, Michaelis-Menten consumption, and no IVR to study steady-state O_2 transport in rat peripheral nerve tissue. They solved the steady-state equations using a finite-difference method and found better agreement with experiment for reduced O_2 supply than in a model with constant O_2 consumption and no axial diffusion. The above model was later extended to time-dependent transport (52). For exponential changes in capillary entrance PO_2, blood velocity, or maximum local O_2 consumption (M_0), they found tissue PO_2 changed either mono- or biexponentially in reaching a new steady state. The slower of the two possible time constants was <0.5 s^{-1}, implying minimal time lag in response of tissue PO_2 to the imposed O_2 supply alterations. Sharma and Jain (80) used a similar model but added terms representing the dynamics of RBC-plasma O_2 flux.

Fletcher and Schubert (19) used a Krogh-type model to show that measured PO_2 histograms in isolated perfused cat heart could be closely matched when axial diffusion was included in the tissue, but only if the diffusion coefficient was 7–10 times the accepted value. This result was not explained by adding tissue Mb (20), even though relatively high Mb concentration and diffusivity (3×10^{-6} cm^2/s) were used. One interpretation of these results is that the Krogh geometry simply does not apply to the heart (see (4,96), discussed below). Hudetz (42) studied O_2 transport in the cerebral cortex using the standard Krogh model but with a conical tissue cylinder that tapered toward the venous end of the capillary. This model did not consider IVR and could be solved analytically. Small increases in O_2 consumption (functional activation) required proportional increases in capillary O_2 supply (blood flow), but large increases in consumption required disproportionate supply increases. For moderate hypoxemia, the predicted increase in blood flow agreed with experimental measurements. Whiteley et al. (95) used a finite-element method to study steady-state O_2 transport from a single axisymmetric capillary. Blood was treated as homogeneous, O_2 consumption was constant, and tissue Mb was included. The main conclusions of this study were that axial diffusion should be included in the tissue and that Mb should be included when tissue PO_2 falls below 13mmHg (assuming $P_{50,Mb}$=2mmHg). Similar previous work using a homogeneous description of blood (33,79) indicated that including Hb-O_2 kinetics lowers end-capillary plasma and tissue PO_2 compared to the equilibrium case, particularly for hypoxia and anemia.

NIH-PA Author Manuscript

McGuire and Secomb (57,58) utilized a Krogh-type model that included IVR, tissue Mb, Michaelis-Menten consumption kinetics, and axial diffusion to study heavily working human skeletal muscle. Right-shifting of the Hb-O_2 dissociation curve (as observed during exercise) and mitochondrial clustering near the capillary were also considered. They showed that there is diffusion limitation and hypoxia in heavily working muscle (58) and predicted capillary densities based on their model and measured parameters (57) . The fact that measured capillary densities are much lower than those predicted suggested that biopsies in contracted muscle lead to underestimates of capillary density (because increased capillary tortuosity is not considered) and do not accurately reflect *in vivo* O_2 transport capacity. Note that heavily working muscle is the case for which the Krogh geometry remains most relevant, since capillary transport is most dominant and parallel capillaries have the least diffusive interaction (see (17,74), discussed below).

NIH-PA Author Manuscript

Multi-Species Models

Krogh-type models have been used to study blood-tissue transport of substances other than O_2; however, here we are concerned principally with O_2 transport and therefore only discuss models in which transport of O_2 is coupled to that of another species. Transport of other species can be important as a means of studying O_2 transport (54) or because of the effect of O_2 on the other species (e.g., O_2-dependent production and consumption of NO (53,84)). Other species can also affect O_2 transport itself; for example, by competing with O_2 for binding to Hb (as does CO), by shifting the Hb-O_2 saturation curve (as discussed below for CO_2), and by inhibiting mitochondrial O_2 consumption (as does NO (53)). Li et al. (54) used a Krogh-type model with four concentric layers (RBCs, plasma, interstitial fluid, and parenchymal cells) to study tracer kinetics of ^{15}O-O_2 and ^{15}O-water. This model considered axial but not radial gradients within each layer (or compartment), as well as exchange between the layers. The steady-state O_2 distribution was first calculated and then used to model coupled dynamics of labeled O_2 and water. By fitting model solutions to experimental tracer curves, this model can be used to estimate myocardial O_2 consumption.

Schacterle et al. (72) developed a simple steady-state model of O_2/CO_2 transport in arterioles surrounded by tissue containing a continuous distribution of capillaries. Blood was treated as homogeneous, and O_2 and CO_2 only interacted through explicit inclusion of the Bohr (CO_2-dependent shifting of Hb-O_2 dissociation curve) and Haldane (O_2-dependent shifting of the Hb-CO_2 dissociation curve) effects. For an arteriole with 22μm diameter and 1000μm length, results suggested that blood PCO_2 comes closer to equilibrium with surrounding tissue than does PO_2. In the study by Dash and Bassingthwaighte (13) a four-layer axially varying model (similar to (54)) was used to study coupled O_2/CO_2 transport between a capillary and the surrounding tissue. The model included bicarbonate and hydrogen ions, and both the Bohr and Haldane effects. This model should require less computation than models that resolve radial gradients and allows calculation of both steady-state and time-dependent transport over a wide range of physiological conditions. Although this model and that of Li et al. (54) did not include radial gradients, the MTCs used between regions could presumably be adjusted to approximate any given situation. The simulation code for this model is available at the Physiome Project website (www.physiome.org/Models/).

Kirkpatrick et al. (47) used a Krogh-type model to study O_2 and glucose transport in tumors. It was shown that glycolysis has only a minor effect on tumor hypoxia but that hypoxia is very sensitive to the O_2 consumption rate. It was also shown that using a distribution of tissue cylinder sizes increases the hypoxic fraction compared with using a single cylinder. Lamkin-Kennard et al. (53) modeled coupled O_2/NO transport in arteriolar cross-sections (no axial transport). Steady-state radial NO and O_2 transport in the lumen, plasma layer, endothelium, vascular wall, and surrounding tissue were simulated for different conditions. One of their principal findings was that increased tissue NO could increase O_2 delivery to more distant tissue regions due to its ability to reversibly inhibit O_2 consumption.

Multi-Vessel Transport Models

Parallel Capillary Models

The above modifications to the standard Krogh model do not consider O_2 diffusion between microvessels, which is believed to be important in many physiological situations. As a first step toward studying O_2 transport by realistic microvascular networks, and in particular to address Krogh model assumptions 6–8 above, parallel arrays of capillaries have been considered. Using data from the hamster cremaster muscle, Klitzman et al. (48) developed a model of steady-state O_2 transport that neglected IVR but included dissolved and Hb-bound O_2 in the blood and diffusion between capillaries (with concurrent blood flow) and tissue in planes perpendicular to the capillary axis. This model, with its square grid of 16 equally spaced capillaries, was solved by Popel et al. (66) using a finite-difference method to study the effect of heterogeneities in O_2 delivery on tissue PO_2 distributions. Using probability distributions to set the RBC supply rate and capillary inlet SO_2, and Michaelis-Menten consumption, it was shown that both mean and minimum tissue PO_2 decreased as the dispersion of these supply parameters increased.

Calculated tissue PO_2 distributions for rest and exercise (~4 times resting O_2 consumption and RBC supply rate) showed general agreement with PO_2 measurements using microelectrodes. Ellsworth et al. (17) used experimental data on the hamster cheek pouch retractor muscle and an extension of the model (66) to study heterogeneity in capillary RBC supply rate, entrance SO_2, and path length. For uniform path lengths, capillary SO_2 became more uniform towards the capillary exit in resting muscle but more heterogeneous in working muscle. However, path length variability resulted in more SO_2 heterogeneity and a closer match with experimental data for the resting case.

Groebe and Thews (32) considered three-dimensional O_2 transport in a single working muscle fiber surrounded by parallel capillaries with increased axial Mb diffusivity. Using an approximate analytical solution that included discrete RBCs inside the capillaries, they showed that a modified Krogh model (including IVR) gave good agreement with their three-dimensional model when the capillary-to-fiber ratio was close to 1, but that both the modified Krogh and Hill models disagreed considerably with their model when the capillary-to-fiber ratio was close to 2. Their model generally agreed with cryospectrophotometric measurements of PO_2 (based on Mb saturation) in working muscle available at the time (21). A simplified version of this model was later presented (29). Hoofd (35,36) presented a steady-state model appropriate for O_2 transport by capillary arrays or networks having a preferential direction, as occurs in skeletal muscle. An analytical solution was first presented for tissue PO_2 in planes perpendicular to the capillaries, and then a numerical method was described for connecting successive planes to obtain the three-dimensional PO_2 distribution. This model included tissue Mb and allowed for variable O_2 consumption, and could be applied to both concurrent and countercurrent flow situations.

Application to dog gracilis muscle (37,38) showed that accurately calculating tissue PO_2 distributions required the inclusion of realistic spacing of parallel capillaries. Since this spacing heterogeneity was not included in (32), much more narrow PO_2 distributions were obtained than in (37,38). Although the model (32) gave good agreement with experimental measurements, these may have underestimated actual tissue PO_2 heterogeneity due to the fact that the spatial resolution was much lower than originally believed, i.e., 60μm vs. <4μm while the mean muscle fiber radius was 45μm (91) .

Salathe (69) presented a method for calculating the steady-state O_2 distribution due to an array of capillaries in the absence of IVR and variable O_2 consumption. The model used matching of average O_2 fluxes and concentrations between neighboring rectangular tissue domains surrounding each capillary to derive a system of ordinary differential equations (for capillary O_2) coupled to a system of algebraic equations (for average tissue domain boundary O_2). This model was later extended to include axial diffusion (70), as well as Mb facilitation and countercurrent flow (83). This model has been applied to arrays of 2–50 capillaries and seems to provide good accuracy (69) and computational efficiency for applicable problems.

Goldman et al. (23) used parallel arrays in a network transport model ((24), see below) to analyze experimental data on capillary hemodynamics and SO_2 in rat skeletal muscle during sepsis (15). Sepsis causes decreased functional capillary density (FCD) and had been found to increase O_2 extraction in capillaries that maintained flow. However, because hemodynamic and SO_2 data could not be obtained from capillaries with RBC velocities greater than 300μm/s, the overall effect of sepsis on tissue O_2 extraction could not be determined. By using a range of “fast-flow” velocities and adjusting the O_2 consumption rate (M_0) to match measured extraction ratios in “normal-flow” vessels, it was shown that consumption increased 2- to 4-fold in sepsis but that tissue hypoxia did not occur. In a subsequent study (22), the baseline model for O_2 transport during sepsis was considered for decreasing O_2 supply. It was shown that the pathological supply dependency seen in sepsis, which had previously been attributed to a defect in arteriolar flow regulation, could be partly explained by further decreases in FCD as flow decreased.

Another approach that has been used in parallel array models of O_2 transport, and which could also be applied to capillary networks, is the Williford-Bruley (W-B) “probabilistic deterministic” numerical method (8,45). This technique uses time-dependent probability density functions in three spatial dimensions to evolve tissue O_2 distributions on a grid. However, it is not clear how features such as tissue Mb and IVR could be treated with the W-B method.

Capillary Network Models

Hsu and Secomb (40) presented a steady-state model of O_2 transport in capillary networks and surrounding tissue based on the Green’s function method. This model included three-dimensional diffusion but not IVR or variable O_2 consumption. The solution method was computationally efficient because it reduced the three-dimensional problem for tissue PO_2 to the one-dimensional problem of finding appropriate source terms for each capillary segment. This model was extended to include variable O_2 consumption (using an iterative procedure) and used to study O_2 transport in mammary adenocarcinoma tumors (76). Using measured microvascular network geometry (Fig. 4) and blood flow, it was shown that O_2 transport was highly heterogeneous and as a result tissue hypoxia occurred at a lower O_2 consumption rate than predicted by the Krogh model for the same average microvessel density. A number of other factors in tumor oxygenation were studied using this model, including the effect of reduced Hb O_2 affinity (46). A version of this model has been used to study O_2 transport in the rat cerebral cortex, using three-dimensional networks reconstructed from micrographs of corrosion casts (75). The three-dimensional network model predicted much lower minimum tissue PO_2 than would an equivalent Krogh model and it was found that hypoxia due to large decreases in blood flow could be avoided by moderate decreases in the O_2 consumption rate. A review and extension of the above Green’s function method was given in (77).

Groebe (30) extended a previous parallel capillary model (32) to the case of three-dimensional O_2 transport from capillary networks. This steady-state model used an approximate analytical solution based on O_2 sources inside individual RBCs and constant O_2 consumption, and included IVR and Mb facilitation. The model was applied to a heavily working muscle fiber supplied by four capillaries and shown to agree with the previous single-fiber results.

Goldman and Popel (24) presented a finite-difference based model that allowed study of O_2 transport by branching networks of microvessels; included three-dimensional diffusion, IVR, Mb facilitation, dissolved and Hb-bound O_2 in the blood; and could calculate steady-state or time-dependent solutions. This model, which also included a two-phase simulation of network blood flow (based on (68)), was used to study the effect of capillary network geometry on steady-state O_2 transport in the hamster cheek pouch retractor muscle. The arrangement of parallel capillaries induced by the underlying geometry of hexagonally packed muscle fibers was found to be important in reducing tissue PO_2 heterogeneity, as was countercurrent flow, and anastomoses between parallel capillaries were found to help maintain blood flow and tissue PO_2 when some parallel capillaries were blocked. The same model was used to study capillary network O_2 transport during oscillatory blood flow or vasomotion (25). A version of this model (using rat parameters) was applied to an expanded microvascular network consisting of 8 capillary modules with feeding arterioles and draining venules (microvascular units, MVUs, Fig. 5) to study the effect of angiogenesis on muscle oxygenation (44). Interestingly, the splitting mode of angiogenesis (increased parallel capillaries) produced the least hypoxia at high O_2 consumption, but also had the highest blood flow; for equal blood flow, the sprouting mode (increased anastomoses) gave the least hypoxia. This complex network model was extended to include plasma Hb (with corresponding RBC-plasma and capillary-tissue MTCs) and used in a combined theoretical/experimental study (87). This work showed that decreased Hb O_2 affinity (P_{50}) can increase diffusive shunting between microvessels and that microvascular structure can affect the Hb affinity needed to minimize tissue hypoxia.

Wieringa et al. (96) presented a three-dimensional network model of steady-state O_2 transport in the heart that assumed constant O_2 consumption and was solved in two-dimensional layers by the finite-element method. Despite a number of simplifications (e.g., no diffusion between layers), this model showed the importance of intercapillary diffusion, particularly when flow direction and path length are heterogeneous, and results indicated that venous PO_2 is not a good indicator of actual tissue oxygenation. Beard and Bassingthwaighte (4) presented a network model of the heart that used 16 parallel capillaries on a hexagonal grid with 160 random cross-connections and included three-dimensional diffusion, Mb facilitation, and Michaelis-Menten consumption.

Using a finite-difference method, they showed that steady-state O_2 distributions were much more heterogeneous than a Krogh-type model would predict and that Mb could reduce tissue hypoxia but only for a modest range of consumption rates. The solution method was extended to an inhomogeneous finite-volume (IVol) method (2) that allowed arbitrary network geometry, time-dependent transport, and larger tissue grid spacing for more efficient numerical solution. The new method was applied to predict PO_2 distributions in perfused hearts based on optical spectroscopy data (5), using a network model as in (4) but with the interstitial space explicitly included (Fig. 6).

Capillary/Arteriole and Venule/Arteriole Interaction Models

To explore experimental data on longitudinal PO_2 gradients in arterioles (50) that suggested the O_2 permeability of blood-perfused tissue was much greater than expected (67), Weerappuli and Popel (94) developed a model of O_2 exchange between an arteriole or venule and surrounding capillary-perfused tissue (resting hamster cheek pouch retractor muscle). This model used a finite-difference method to solve the steady-state problem in the plane perpendicular to the arteriole with a continuous description of capillary O_2 transport (71). Results were obtained for 1^{st} and 4^{th} order arterioles with constant luminal PO_2 values of 37.7 and 31.6 mmHg, respectively, and a far-field tissue PO_2 of 20mmHg. Results for Sherwood number (Sh, dimensionless O_2 flux) vs. Pe showed increases up to ~Pe=30. There was a wake of increased tissue PO_2 on the downstream side of the arteriole and slightly greater flux from the larger arteriole. A venule with luminal PO_2 of 15mmHg had a similar but opposite effect on nearby tissue PO_2. Further work using this model (93) again suggested that the O_2 permeability *in vivo* must be 1–2 orders of magnitude greater than the *in vitro* value (i.e., the Krogh constant, K=Dα).

To address possible errors caused by using a continuous description of capillary O_2 transport, Hsu and Secomb (39) applied the Green's function method to O_2 transport from a single arteriole perpendicular to a plane containing several parallel discrete capillaries. They found arteriolar O_2 flux of the same magnitude as (93), but with a slower increase as a function of Pe. Hence, the controversy over the actual magnitudes of arteriolar O_2 flux and *in vivo* O_2 permeability remained unresolved. Tsai et al. (86) proposed that extremely high arteriolar wall O_2 consumption (see discussion of their methods in (26)) was causing the discrepancy between theory and experiment, but an analysis of available data based on the O_2 diffusion and consumption properties of the wall (89) concluded that O_2 fluxes had been overestimated based on estimates of convective O_2 transport at upstream and downstream points.

Despite the above controversy, a version of the model (39) was used to investigate details of three-dimensional capillary-arteriole O_2 exchange in a block of tissue containing parallel capillaries crossed by two arterioles. This study (74) gave an indication of the roles that capillaries and arterioles play in O_2 transport under realistic conditions. For resting conditions, diffusive O_2 loss from arterioles was 86% of total consumption, but more than half this O_2 was taken up by capillaries and delivered to other locations. During exercise (10 times resting O_2 consumption and blood flow), the diffusive O_2 loss from arterioles was 32% of total consumption and only 5% of the total consumed O_2 diffused from arterioles into capillaries. Thus, arterioles supplied about 40% of consumed O_2 directly to tissue during rest and 27% during exercise.

Chen et al. (9) used a steady-state three-dimensional model to study coupled NO/O_2 transport in an arteriole/venule pair surrounded by capillary-perfused tissue, which was modeled as a porous medium that connected the larger vessels by both diffusion and convection. Capillaries facilitated the release of O_2 from the larger vessel pair to the surrounding tissue and greatly enhanced transport of NO from venule to arteriole. The finding of increased O_2 release might help explain the experimental finding of large arteriolar O_2 efflux (50,67); however, this was measured in unbranched vessels whereas (9) included O_2 convection through the arteriolar wall.

Conclusions and Future Directions

From the many detailed theoretical studies performed over the last two decades, a number of important results on microvascular O_2 transport have emerged. The importance of biophysical properties (Krogh assumptions 1–5) was first evaluated, while later work examined the significance of geometric and hemodynamic properties of the microvasculature (assumptions 6–8). In particular, the effects of heterogeneities in capillary spacing, O_2 supply, flow direction, and path length, as well as the way in which arterioles and venules interact with capillaries and tissue, have only begun to be understood as more sophisticated models have been developed. There is still far from a complete understanding of how a particular functional microvascular structure (geometry, hemodynamics, inlet SO_2) determines tissue oxygenation and O_2 consumption. In addition, the effect of realistic temporal variations in O_2 supply on three-dimensional O_2 transport to tissue is largely unknown.

Although more efficient methods of including the effect of capillary-scale heterogeneities on organ-scale physiology are still needed, existing theoretical models are capable of investigating most outstanding details of structure-function relationships in microvascular O_2 transport. To support this work, detailed experimental data is needed to determine input parameters and thoroughly validate the models (which for the most part has never been done). Experimental methods have for some time been less developed than theoretical ones, as pointed out by Pittman (64); however, a combination of existing and emerging techniques (1,26,43,81,85,90) shows promise for supporting further theoretical advances based on development and validation of realistic models of *in vivo* O_2 transport. One important area of current theoretical modeling of the microcirculation involves multi-scale models that couple details of O_2 transport to related biological processes (such as angiogenesis (56) and metabolism (3)) occurring at similar and smaller scales. Combined with more fundamental studies of microvascular O_2 transport, these multi-scale models should lead to a more complete picture of the synergy between tissue properties and functional characteristics of the microvasculature, and this could have dramatic implications both for maintenance of health and treatment of various diseases.

Acknowledgments

The author would like to thank the editors of this special issue, particularly Dr. Timothy Secomb. Research assistance was provided by Ms. Meaghan MacKie, and this work was supported by grants from the Canadian Institutes of Health Research (MOP-49541, MOP-81344) and the National Institutes of Health (HL089125).

Grants: Canadian Institutes of Health Research (MOP-49541, MOP-81344)

National Institutes of Health (HL089125)

References

1. Bakalova R. Ultra-fast biosensors and multi-photon microscopy in the future of brain studies. Cell Mol Neurobiol 2007;27:359–365. [PubMed: 17186362]
2. Beard DA. Computational framework for generating transport models from databases of microvascular anatomy. Ann Biomed Eng 2001;29:837–843. [PubMed: 11764314]
3. Beard DA. Modeling of oxygen transport and cellular energetics explains observations on in vivo cardiac energy metabolism. PLoS Comput Biol 2006;2:e107. [PubMed: 16978045]
4. Beard DA, Bassingthwaighte JB. Modeling advection and diffusion of oxygen in complex vascular networks. Ann Biomed Eng 2001;29:298–310. [PubMed: 11339327]
5. Beard DA, Schenkman KA, Feigl EO. Myocardial oxygenation in isolated hearts predicted by an anatomically realistic microvascular transport model. Am J Physiol Heart Circ Physiol 2003;285:H1826–H1836. [PubMed: 12869375]
6. Bos C, Hoofd L, Oostendorp T. The effect of separate red blood cells on capillary tissue oxygenation calculated with a numerical model. IMA J Math Appl Med Biol 1996;13:259–274. [PubMed: 8968786]
7. Bos C, Hoofd L, Oostendorp T. Mathematical model of erythrocytes as point-like sources. Math Biosci 1995;125:165–189. [PubMed: 7881193]
8. Bruley DF. Modeling oxygen transport: development of methods and current state. Adv Exp Med Biol 1994;345:33–42. [PubMed: 8079726]
9. Chen X, Buerk DG, Barbee KA, Jaron D. A model of NO/O2 transport in capillary-perfused tissue containing an arteriole and venule pair. Ann Biomed Eng 2007;35:517–529. [PubMed: 17235703]
10. Clark A Jr, Federspiel WJ, Clark PA, Cokelet GR. Oxygen delivery from red cells. Biophys J 1985;47:171–181. [PubMed: 3978198]
11. Cole RH, Vandegriff KD, Szeri AJ, Savas O, Baker DA, Winslow RM. A quantitative framework for the design of acellular hemoglobins as blood substitutes: implications of dynamic flow conditions. Biophys Chem 2007;128:63–74. [PubMed: 17418478]
12. Dash RK, Bassingthwaighte JB. Blood HbO2 and HbCO2 dissociation curves at varied O2, CO2, pH, 2,3-DPG and temperature levels. Ann Biomed Eng 2004;32:1676–1693. [PubMed: 15682524]
13. Dash RK, Bassingthwaighte JB. Simultaneous blood-tissue exchange of oxygen, carbon dioxide, bicarbonate, and hydrogen ion. Ann Biomed Eng 2006;34:1129–1148. [PubMed: 16775761]
14. Eggleton CD, Vadapalli A, Roy TK, Popel AS. Calculations of intracapillary oxygen tension distributions in muscle. Math Biosci 2000;167:123–143. [PubMed: 10998485]
15. Ellis CG, Bateman RM, Sharpe MD, Sibbald WJ, Gill R. Effect of a maldistribution of microvascular blood flow on capillary O2 extraction in sepsis. Am J Physiol Heart Circ Physiol 2002;282:H156–H164. [PubMed: 11748059]
16. Ellis CG, Ellsworth ML, Pittman RN. Determination of red blood cell oxygenation in vivo by dual video densitometric image analysis. Am J Physiol 1990;258:H1216–H1223. [PubMed: 2331009]
17. Ellsworth ML, Popel AS, Pittman RN. Assessment and impact of heterogeneities of convective oxygen transport parameters in capillaries of striated muscle: experimental and theoretical. Microvasc Res 1988;35:341–362. [PubMed: 3393095]

18. Federspiel WJ, Popel AS. A theoretical analysis of the effect of the particulate nature of blood on oxygen release in capillaries. Microvasc Res 1986;32:164–189. [PubMed: 3762425]
19. Fletcher JE, Schubert RW. Axial diffusion and wall permeability effects in perfused capillary-tissue structures. Biosystems 1987;20:153–174. [PubMed: 3607274]
20. Gardner JD, Schubert RW. Evaluation of myoglobin function in the presence of axial diffusion. Adv Exp Med Biol 1997;411:157–169. [PubMed: 9269424]
21. Gayeski TE, Honig CR. O2 gradients from sarcolemma to cell interior in red muscle at maximal VO2. Am J Physiol 1986;251:H789–H799. [PubMed: 3766756]
22. Goldman D, Bateman RM, Ellis CG. Effect of decreased O2 supply on skeletal muscle oxygenation and O2 consumption during sepsis: role of heterogeneous capillary spacing and blood flow. Am J Physiol Heart Circ Physiol 2006;290:H2277–H2285. [PubMed: 16399873]
23. Goldman D, Bateman RM, Ellis CG. Effect of sepsis on skeletal muscle oxygen consumption and tissue oxygenation: interpreting capillary oxygen transport data using a mathematical model. Am J Physiol Heart Circ Physiol 2004;287:H2535–H2544. [PubMed: 15319199]
24. Goldman D, Popel AS. A computational study of the effect of capillary network anastomoses and tortuosity on oxygen transport. J Theor Biol 2000;206:181–194. [PubMed: 10966756]
25. Goldman D, Popel AS. A computational study of the effect of vasomotion on oxygen transport from capillary networks. J Theor Biol 2001;209:189–199. [PubMed: 11401461]
26. Golub AS, Barker MC, Pittman RN. PO2 profiles near arterioles and tissue oxygen consumption in rat mesentery. Am J Physiol Heart Circ Physiol 2007;293:H1097–H1106. [PubMed: 17483242]
27. Golub AS, Popel AS, Zheng L, Pittman RN. Analysis of phosphorescence in heterogeneous systems using distributions of quencher concentration. Biophys J 1997;73:452–465. [PubMed: 9199808]
28. Greene AS, Tonellato PJ, Zhang Z, Lombard JH, Cowley AW Jr. Effect of microvascular rarefaction on tissue oxygen delivery in hypertension. Am J Physiol 1992;262:H1486–H1493. [PubMed: 1590452]
29. GroebeKAn easy-to-use model for O2 supply to red muscleValidity of assumptions, sensitivity to errors in data. Biophys J19956812461269 [PubMed: 7787016]
30. Groebe K. A versatile model of steady state O2 supply to tissue. Application to skeletal muscle. Biophys J 1990;57:485–498. [PubMed: 2306498]
31. Groebe K, Thews G. Effects of red cell spacing and red cell movement upon oxygen release under conditions of maximally working skeletal muscle. Adv Exp Med Biol 1989;248:175–185. [PubMed: 2782144]
32. Groebe K, Thews G. Role of geometry and anisotropic diffusion for modelling PO2 profiles in working red muscle. Respir Physiol 1990;79:255–278. [PubMed: 2356363]
33. Gutierrez G. The rate of oxygen release and its effect on capillary O2 tension: a mathematical analysis. Respir Physiol 1986;63:79–96. [PubMed: 3952387]
34. Hellums JD, Nair PK, Huang NS, Ohshima N. Simulation of intraluminal gas transport processes in the microcirculation. Ann Biomed Eng 1996;24:1–24. [PubMed: 8669708]
35. Hoofd L. Calculation of oxygen pressures in tissue with anisotropic capillary orientation. I. Two-dimensional analytical solution for arbitrary capillary characteristics. Math Biosci 1995;129:1–23. [PubMed: 7670223]
36. Hoofd L. Calculation of oxygen pressures in tissue with anisotropic capillary orientation. II. Coupling of two-dimensional planes. Math Biosci 1995;129:25–39. [PubMed: 7670224]
37. Hoofd L, Turek Z. Effect of realistic capillary spacing on pO2 calculations in dog gracilis muscle. Med Biol Eng Comput 1994;32:436–439. [PubMed: 7967811]
38. Hoofd L, Turek Z. Realistic modelling of capillary spacing in dog gracilis muscle greatly influences the heterogeneity of calculated tissue oxygen pressures. Adv Exp Med Biol 1996;388:333–340. [PubMed: 8798831]
39. Hsu R, Secomb TW. Analysis of oxygen exchange between arterioles and surrounding capillary-perfused tissue. J Biomech Eng 1992;114:227–231. [PubMed: 1602766]
40. Hsu R, Secomb TW. A Green's function method for analysis of oxygen delivery to tissue by microvascular networks. Math Biosci 1989;96:61–78. [PubMed: 2520192]

41. Huang NS, Hellums JD. A theoretical model for gas transport and acid/base regulation by blood flowing in microvessels. Microvasc Res 1994;48:364–388. [PubMed: 7731399]

42. Hudetz AG. Mathematical model of oxygen transport in the cerebral cortex. Brain Res 1999;817:75–83. [PubMed: 9889326]

43. Japee SA, Pittman RN, Ellis CG. A new video image analysis system to study red blood cell dynamics and oxygenation in capillary networks. Microcirculation 2005;12:489–506. [PubMed: 16147466]

44. Ji JW, Tsoukias NM, Goldman D, Popel AS. A computational model of oxygen transport in skeletal muscle for sprouting and splitting modes of angiogenesis. J Theor Biol 2006;241:94–108. [PubMed: 16388825]

45. Kang KA, Bruley DF, Bicher H. A computer simulation of simultaneous heat and oxygen transport during heterogeneous three dimensional tumor hyperthermia. Adv Exp Med Biol 1988;222:747–756. [PubMed: 3364302]

46. Kavanagh BD, Secomb TW, Hsu R, Lin PS, Venitz J, Dewhirst MW. A theoretical model for the effects of reduced hemoglobin-oxygen affinity on tumor oxygenation. Int J Radiat Oncol Biol Phys 2002;53:172–179. [PubMed: 12007957]

47. Kirkpatrick JP, Brizel DM, Dewhirst MW. A mathematical model of tumor oxygen and glucose mass transport and metabolism with complex reaction kinetics. Radiat Res 2003;159:336–344. [PubMed: 12600236]

48. Klitzman B, Popel AS, Duling BR. Oxygen transport in resting and contracting hamster cremaster muscles: experimental and theoretical microvascular studies. Microvasc Res 1983;25:108–131. [PubMed: 6835096]

49. Krogh A. The number and distribution of capillaries in muscles with calculations of the oxygen pressure head necessary for supplying the tissue. J Physiol 1919;52:409–415. [PubMed: 16993405]

50. Kuo L, Pittman RN. Effect of hemodilution on oxygen transport in arteriolar networks of hamster striated muscle. Am J Physiol 1988;254:H331–H339. [PubMed: 3344823]

51. Lagerlund TD, Low PA. Axial diffusion and Michaelis-Menten kinetics in oxygen delivery in rat peripheral nerve. Am J Physiol 1991;260:R430–R440. [PubMed: 1996727]

52. Lagerlund TD, Low PA. Mathematical modeling of time-dependent oxygen transport in rat peripheral nerve. Comput Biol Med 1993;23:29–47. [PubMed: 8467637]

53. Lamkin-Kennard KA, Buerk DG, Jaron D. Interactions between NO and O2 in the microcirculation: a mathematical analysis. Microvasc Res 2004;68:38–50. [PubMed: 15219419]

54. Li Z, Yipintsoi T, Bassingthwaighte JB. Nonlinear model for capillary-tissue oxygen transport and metabolism. Ann Biomed Eng 1997;25:604–619. [PubMed: 9236974]

55. Lin PC, Kreutzer U, Jue T. Anisotropy and temperature dependence of myoglobin translational diffusion in myocardium: implication for oxygen transport and cellular architecture. Biophys J 2007;92:2608–2620. [PubMed: 17218454]

56. Mac, Gabhann F.; Ji, JW.; Popel, AS. Multi-scale computational models of pro-angiogenic treatments in peripheral arterial disease. Ann Biomed Eng 2007;35:982–994. [PubMed: 17436110]

57. McGuire BJ, Secomb TW. Estimation of capillary density in human skeletal muscle based on maximal oxygen consumption rates. Am J Physiol Heart Circ Physiol 2003;285:H2382–H2391. [PubMed: 12893642]

58. McGuire BJ, Secomb TW. A theoretical model for oxygen transport in skeletal muscle under conditions of high oxygen demand. J Appl Physiol 2001;91:2255–2265. [PubMed: 11641369]

59. Nair PK, Hellums JD, Olson JS. Prediction of oxygen transport rates in blood flowing in large capillaries. Microvasc Res 1989;38:269–285. [PubMed: 2607997]

60. Nair PK, Huang NS, Hellums JD, Olson JS. A simple model for prediction of oxygen transport rates by flowing blood in large capillaries. Microvasc Res 1990;39:203–211. [PubMed: 2352490]

61. Page TC, Light WR, Hellums JD. Prediction of microcirculatory oxygen transport by erythrocyte/hemoglobin solution mixtures. Microvasc Res 1998;56:113–126. [PubMed: 9756734]

62. Papadopoulos S, Endeward V, Revesz-Walker B, Jurgens KD, Gros G. Radial and longitudinal diffusion of myoglobin in single living heart and skeletal muscle cells. Proc Natl Acad Sci U S A 2001;98:5904–5909. [PubMed: 11320218]

63. Piiper J, Scheid P. Diffusion limitation of O2 supply to tissue in homogeneous and heterogeneous models. Respir Physiol 1991;85:127–136. [PubMed: 1947449]
64. Pittman RN. Oxygen transport and exchange in the microcirculation. Microcirculation 2005;12:59–70. [PubMed: 15804974]
65. Popel AS. Theory of oxygen transport to tissue. Crit Rev Biomed Eng 1989;17:257–321. [PubMed: 2673661]
66. Popel AS, Charny CK, Dvinsky AS. Effect of heterogeneous oxygen delivery on the oxygen distribution in skeletal muscle. Math Biosci 1986;81:91–113.
67. Popel AS, Pittman RN, Ellsworth ML. Rate of oxygen loss from arterioles is an order of magnitude higher than expected. Am J Physiol 1989;256:H921–H924. [PubMed: 2923247]
68. Pries AR, Secomb TW, Gaehtgens P, Gross JF. Blood flow in microvascular networks. Experiments and simulation. Circ Res 1990;67:826–834. [PubMed: 2208609]
69. Salathe EP. Mathematical analysis of oxygen concentration in a two dimensional array of capillaries. J Math Biol 2003;46:287–308. [PubMed: 12673508]
70. Salathe EP. A mathematical method for determining oxygen distribution in skeletal muscle with multiple capillaries and axial diffusion. Proc R Soc Lond A Math Phys Eng 2005;461:975–1004.
71. Salathe EP. Mathematical modeling of oxygen transport in skeletal muscle. Math Biosci 1982;58:171–184.
72. Schacterle RS, Adams JM, Ribando RJ. A theoretical model of gas transport between arterioles and tissue. Microvasc Res 1991;41:210–228. [PubMed: 1904978]
73. Schumacker PT, Samsel RW. Analysis of oxygen delivery and uptake relationships in the Krogh tissue model. J Appl Physiol 1989;67:1234–1244. [PubMed: 2793716]
74. Secomb TW, Hsu R. Simulation of O2 transport in skeletal muscle: diffusive exchange between arterioles and capillaries. Am J Physiol Heart Circ Physiol 1994;267:H1214–H1221.
75. Secomb TW, Hsu R, Beamer NB, Coull BM. Theoretical simulation of oxygen transport to brain by networks of microvessels: effects of oxygen supply and demand on tissue hypoxia. Microcirculation 2000;7:237–247. [PubMed: 10963629]
76. Secomb TW, Hsu R, Dewhirst MW, Klitzman B, Gross JF. Analysis of oxygen transport to tumor tissue by microvascular networks. Int J Radiat Oncol Biol Phys 1993;25:481–489. [PubMed: 8436527]
77. Secomb TW, Hsu R, Park EY, Dewhirst MW. Green's function methods for analysis of oxygen delivery to tissue by microvascular networks. Ann Biomed Eng 2004;32:1519–1529. [PubMed: 15636112]
78. Sharan M, Jones MD Jr, Koehler RC, Traystman RJ, Popel AS. A compartmental model for oxygen transport in brain microcirculation. Ann Biomed Eng 1989;17:13–38. [PubMed: 2919811]
79. Sharan M, Selvakumar S. The effects of chemical kinetics on oxygen delivery to tissue. Math Biosci 1992;108:253–277. [PubMed: 1547365]
80. Sharma GC, Jain M. A computational solution of mathematical model for oxygen transport in peripheral nerve. Comput Biol Med 2004;34:633–645. [PubMed: 15369713]
81. Styp-Rekowska B, Disassa NM, Reglin B, Ulm L, Kuppe H, Secomb TW, Pries AR. An imaging spectroscopy approach for measurement of oxygen saturation and hematocrit during intravital microscopy. Microcirculation 2007;14:207–221. [PubMed: 17454673]
82. Sullivan JP, Gordon JE, Palmer AF. Simulation of oxygen carrier mediated oxygen transport to C3A hepatoma cells housed within a hollow fiber bioreactor. Biotechnol Bioeng 2006;93:306–317. [PubMed: 16161160]
83. Teboh-Ewungkem MI, Salathe EP. The role of counter-current exchange in preventing hypoxia in skeletal muscle. Bull Math Biol 2006;68:2191–2204. [PubMed: 17086494]
84. Thomas DD, Liu X, Kantrow SP, Lancaster JR Jr. The biological lifetime of nitric oxide: implications for the perivascular dynamics of NO and O2. Proc Natl Acad Sci U S A 2001;98:355–360. [PubMed: 11134509]
85. Tozer GM, Ameer-Beg SM, Baker J, Barber PR, Hill SA, Hodgkiss RJ, Locke R, Prise VE, Wilson I, Vojnovic B. Intravital imaging of tumour vascular networks using multi-photon fluorescence microscopy. Adv Drug Deliv Rev 2005;57:135–152. [PubMed: 15518926]

86. Tsai AG, Friesenecker B, Mazzoni MC, Kerger H, Buerk DG, Johnson PC, Intaglietta M. Microvascular and tissue oxygen gradients in the rat mesentery. Proc Natl Acad Sci U S A 1998;95:6590–6595. [PubMed: 9618456]
87. Tsoukias NM, Goldman D, Vadapalli A, Pittman RN, Popel AS. A computational model of oxygen delivery by hemoglobin-based oxygen carriers in three-dimensional microvascular networks. J Theor Biol 2007;248:657–674. [PubMed: 17686494]
88. Vadapalli A, Goldman D, Popel AS. Calculations of oxygen transport by red blood cells and hemoglobin solutions in capillaries. Artif Cells Blood Substit Immobil Biotechnol 2002;30:157–188. [PubMed: 12066873]
89. Vadapalli A, Pittman RN, Popel AS. Estimating oxygen transport resistance of the microvascular wall. Am J Physiol Heart Circ Physiol 2000;279:H657–H671. [PubMed: 10924065]
90. Varghese HJ, MacKenzie LT, Groom AC, Ellis CG, Chambers AF, MacDonald IC. Mapping of the functional microcirculation in vital organs using contrast-enhanced in vivo video microscopy. Am J Physiol Heart Circ Physiol 2005;288:H185–H193. [PubMed: 15388500]
91. Voter WA, Gayeski TE. Determination of myoglobin saturation of frozen specimens using a reflecting cryospectrophotometer. Am J Physiol 1995;269:H1328–H1341. [PubMed: 7485565]
92. Wang CH, Popel AS. Effect of red blood cell shape on oxygen transport in capillaries. Math Biosci 1993;116:89–110. [PubMed: 8343620]
93. Weerappuli DP, Pittman RN, Popel AS. Effect of convection in capillaries on oxygen removal from arterioles in striated muscle. J Theor Biol 1990;147:275–288. [PubMed: 2277509]
94. Weerappuli DP, Popel AS. A model of oxygen exchange between an arteriole or venule and the surrounding tissue. J Biomech Eng 1989;111:24–31. [PubMed: 2747229]
95. Whiteley JP, Gavaghan DJ, Hahn CE. Mathematical modelling of oxygen transport to tissue. J Math Biol 2002;44:503–522. [PubMed: 12111100]
96. Wieringa PA, Stassen HG, Van Kan JJ, Spaan JA. Oxygen diffusion in a network model of the myocardial microcirculation. Int J Microcirc Clin Exp 1993;13:137–169. [PubMed: 8307707]

NIH-PA Author Manuscript
NIH-PA Author Manuscript

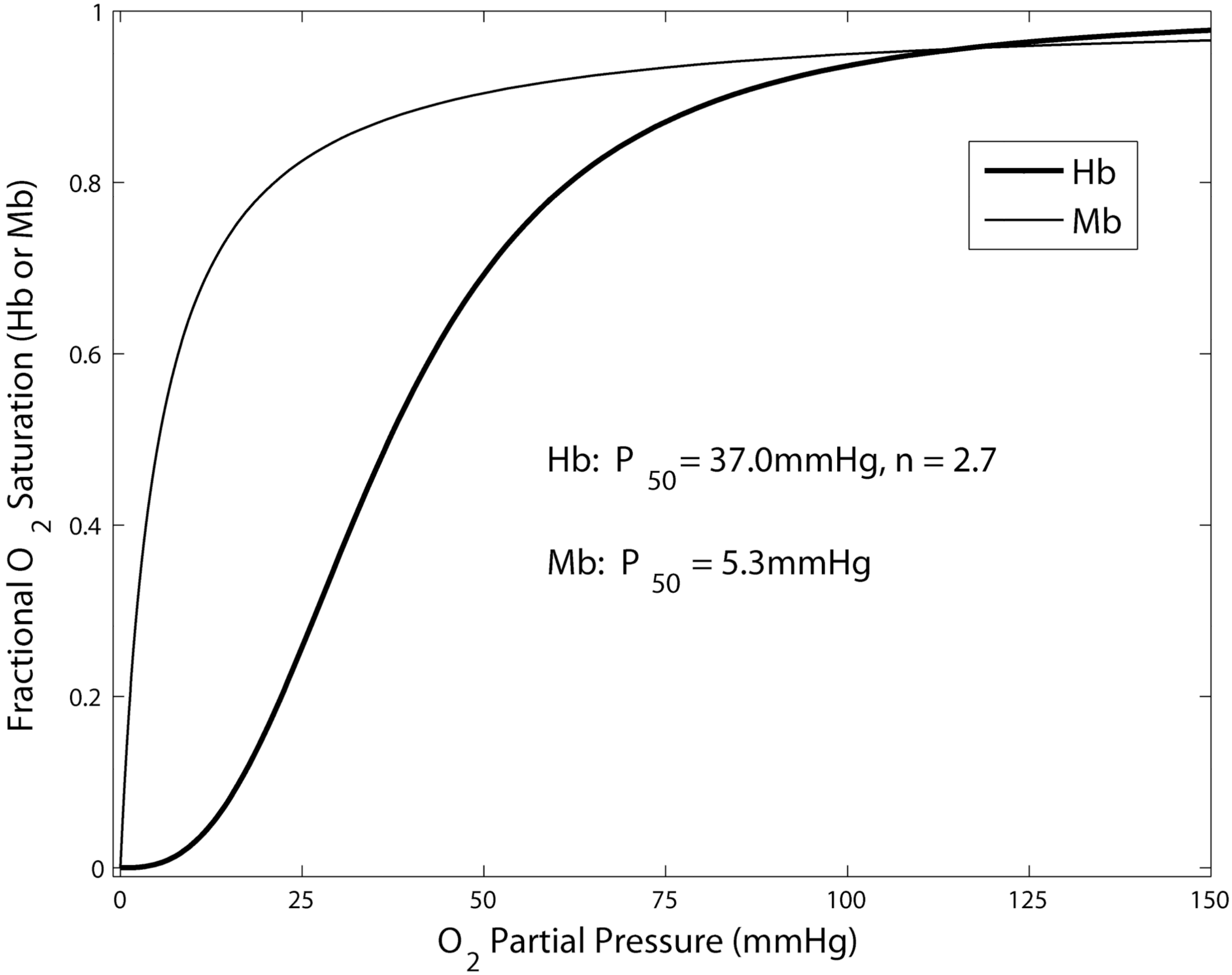

Figure 1.
Equilibrium dissociation curves for fractional Hb-O_2 and Mb-O_2 binding as a function of PO_2. Parameter values shown are typical for rat blood.

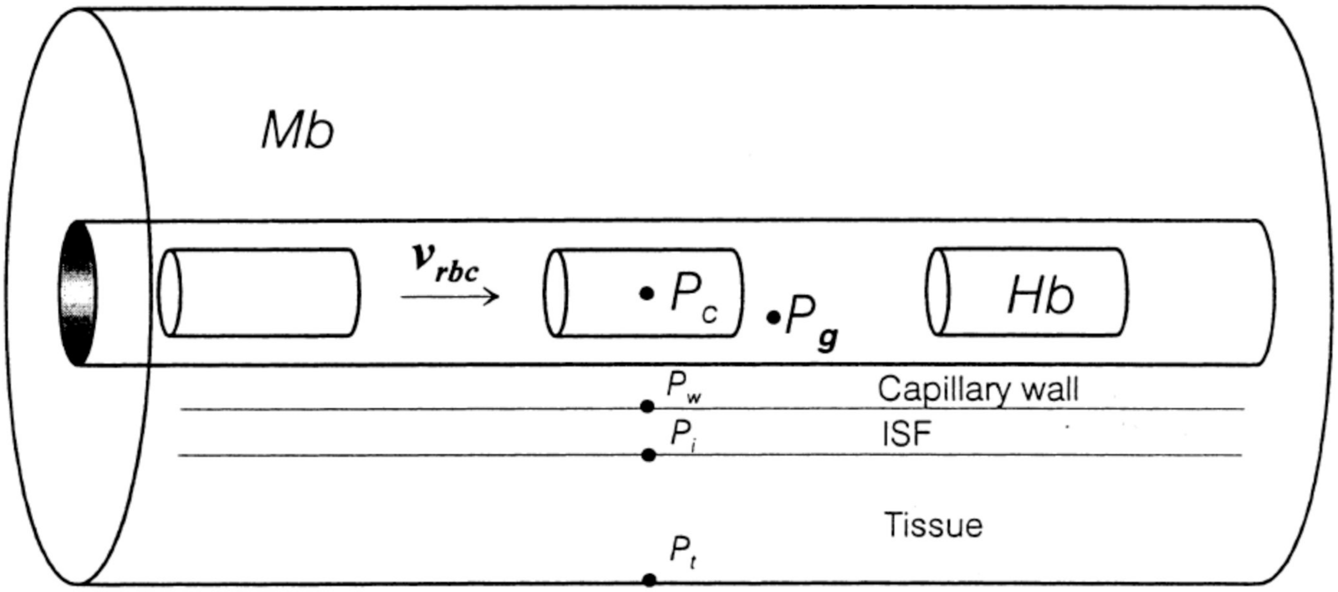

Figure 2.
Axially symmetric geometry and cylindrical RBCs used to calculate capillary MTCs. Reprinted from Eggleton et al. (14) with permission.

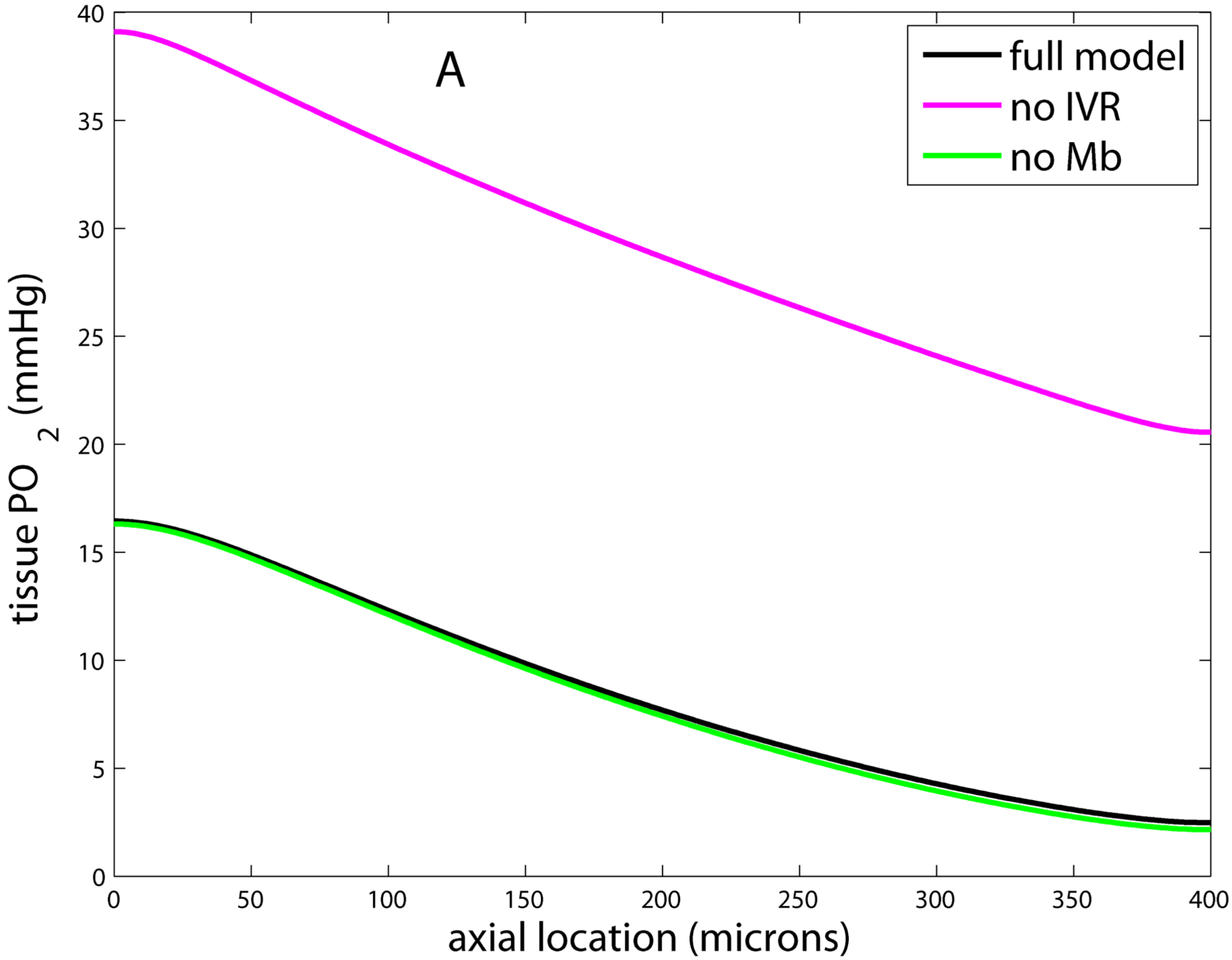

Figure 3.

Effects of neglecting features i–iv in modified Krogh models. Shown is PO_2 at tissue edge ($r=R_t$) vs. axial location (z) for full model that includes Michaelis-Menten consumption, intravascular resistance, Mb facilitation, and axial diffusion in the tissue; and models that neglect one of these. A: Model without IVR has tissue PO_2 about 25mmHg higher than full model, while model without Mb has slightly lower PO_2 in lethal corner. B: Model with constant consumption has lower PO_2 at all locations and gives zero PO_2 for last 50μm, while model with no axial diffusion has higher PO_2 at arterial end and lower PO_2 at venous end.

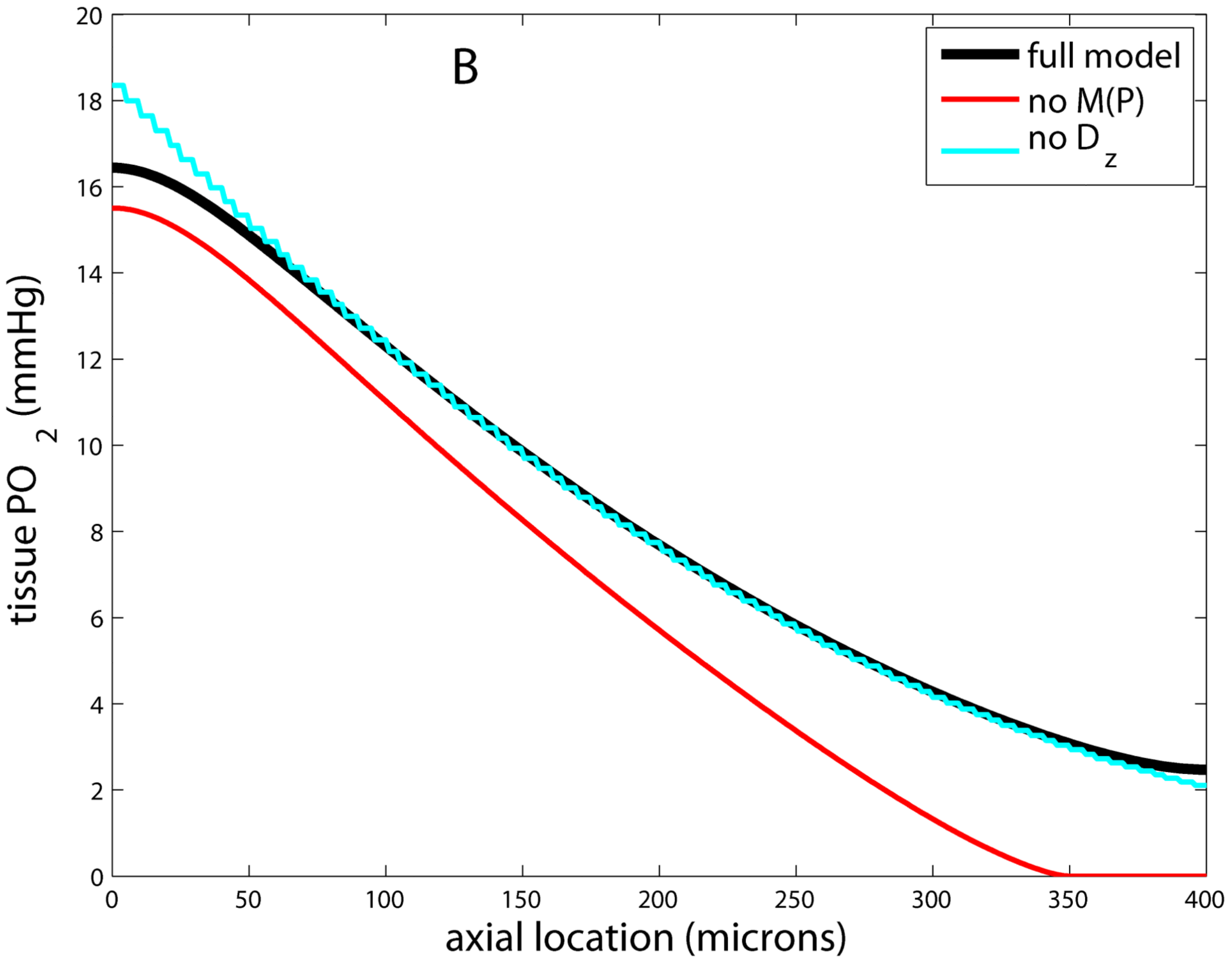

Figure 4.
Geometry of microvascular network used to study O_2 transport in tumors. Reprinted from Kavanagh et al. (46) with permission.

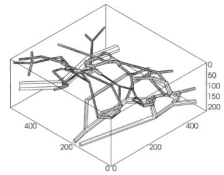

Figure 5.

Geometry of a skeletal muscle microvascular unit containing two capillary networks with supplying arterioles and draining venules. Single and multiple MVUs have been considered in O_2 transport studies of angiogenesis (44) and Hb-based blood substitutes (87). Reprinted from Tsoukias et al. (87) with permission.

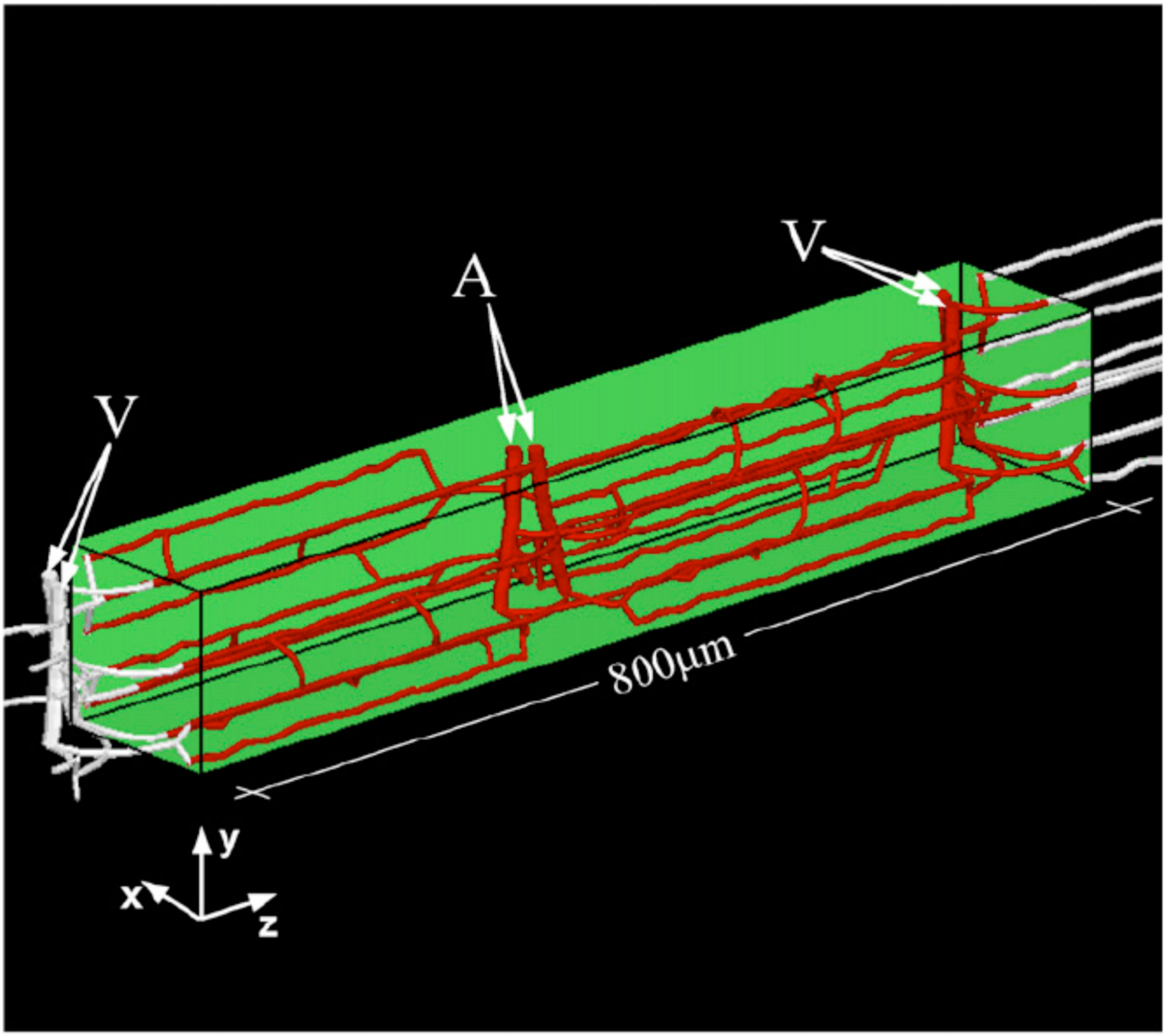

Figure 6.
Geometry of capillary network (red), muscle fibers (grey), and interstitial space (white) used to study O_2 transport in the heart. Reprinted from Beard et al. (5) with permission.

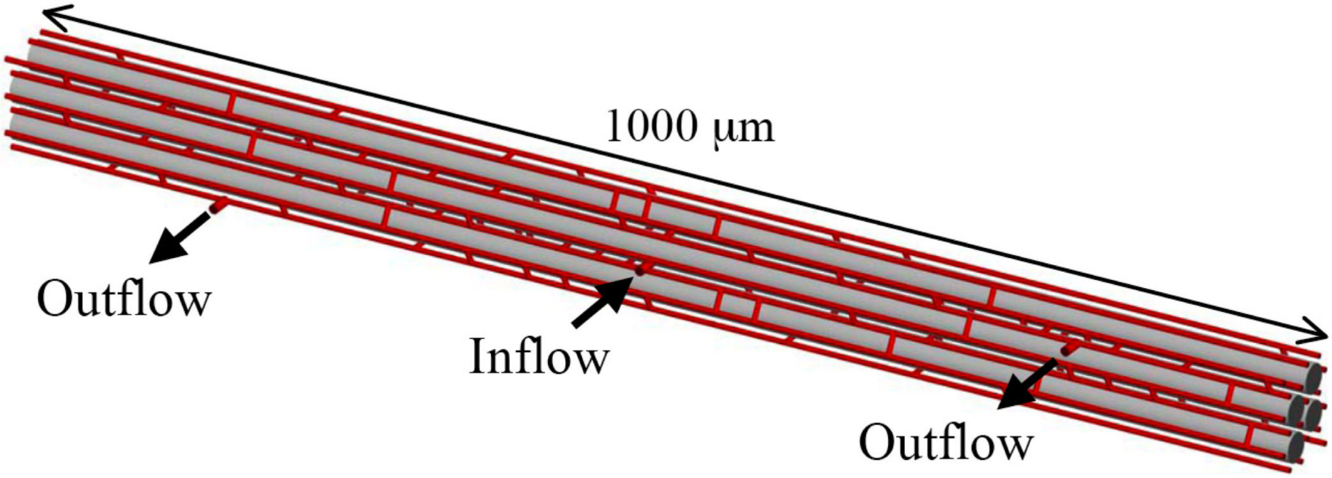

Figure 7.